Mitsui J, Mizuta I, Toyoda A, Ashida R, Takahashi Y, Goto J, Fukuda Y, Date H, Iwata A, Yamamoto M, Hattori N, Murata M, Toda T, Tsuji S.	Mutations for Gaucher disease confer a high susceptibility to Parkinson disease.	Arch Neurol	in press		
Shikishima C, Hiraishi K, Yamagata S, Sugimoto Y, Takemura R, Ozaki K, Okada M, Toda T, Ando J.	Is g an entity? A Japanese twin study using syllogisms and intelligence tests.	Intelligence	in press		
Murata M.	Levodopa in the early treatment of Parkinson's disease	Parkinsonism & Related Disorders	15(1)	S17-S20	2009
Asanuma M, Miyazaki I, Diaz-Corrales FJ, Miyoshi K, Ogawa N, Murata M.	Preventing effects of a novel anti-parkinsonian agent zonisamide on dopamine quinine formation.	Neurosci Res.	60	106-113	2008
Ota M, Sato N, Saito Y, Endo F, Murata M, Asada T.	Diffusion tensor imaging in familial spastic paraplegia with mental impairment and thin corpus callosum.	Magn Reson Med Sci,	7(3)	163-167	2008
Okamoto T, Ogawa M, Lin Y, Murata M, Miyake S, Ymamura T.	Treatment of neuromyelitis opica: Current debate.	Ther Adv Neurol Disord	1	43-52	2008
Kobayashi A, Arima K, Ogawa M, Murata M.	Plaque-type deposition of prion Protein in the damaged white matter of sporadic Creutzfeldt-Jakob disease MM1 patients.	Acta Neuropathol	116	561-566	2008
Ning Y, Kanai K, Tomiyama H, Li Y, Funayama M, Yoshino H, Sato S, Asahina M, Kuwabara S, Takeda A, Hattori T.	PARK9-linked parkinsonism in Eastern Asia: Mutation detection in ATP13A2 and clinical phenotype.	Neurology	70	1491-1493	2008

Ross OA, Wu YR, Lee MC, Funayama M, Chen ML, Soto AI, Mata IF, Lee-Chen GJ, Chen CM, Tang M, Zhao Y, Hattori N, Farrer MJ, Tan EK, Wu RM.	Analysis of Lrrk2 R1628P as a risk factor for Parkinson's disease.	Ann Neurol	64	88-92	2008
Funayama M, Li Y, Tsoi TH, Lam CW, Ohi T, Yazawa S, Uyama E, Djaldetti R, Melamed E, Yoshino H, Imamichi Y, Takashima H, Nishioka K, Sato K, Tomiyama H, Kubo S, MD, Mizuno Y, Hattori N.	Familial parkinsonism with digenic *parkin* and *PINK1* mutations.	Mov Disord.	23	1461-1465	2008
Tomiyama H, Kokubo Y, Sasaki R, Li Y, Imamichi Y, Funayama M, Mizuno Y, Hattori N, Kuzuhara S.	Mutation analyses in amyotrophic lateral sclerosis/parkinsonism-dementia complex of the Kii peninsula, Japan.	Mov Disord.	23	2344-2348	2008
Mellick GD, Siebert GA, Funayama M, Buchanan DD, Li Y, Imamichi Y, Yoshino H, Silburn PA, Hattori N.	Screening PARK Genes for Mutations in Early Onset Parkinson's Disease Patients from Queensland, Australia.	Parkinsonism & Related Disorders	15	105-109	2009
Momma K, Funayama M, Li Y, Ichinose H, Motoyoshi K, Hattori N, Mizuno Y, Kamakura K.	A new mutation in the GCH1 gene presents as early-onset Parkinsonism.	Parkinsonism & Related Disorders	15	160-161	2009

Ross, OA, Braithwaite, AT, Skipper, LM, Kachergus, J, Hulihan, MM, Middleton, FA et al.	Genomic investigation of alpha-synuclein multiplication and parkinsonism.	Ann Neurol	63	743-750	2008
Mizuno Y, Hattori N, Kubo SI, Sato S, Nishioka K, Hatano T, Tomiyama H, Funayama M, Machida Y, Mochizuki H.	Progress in the pathogenesis and genetics of Parkinson's disease.	Philos Trans R Soc Lond B Biol Sci.	363	2215-2227	2008
戸田達史	福山型筋ジストロフィー	ビジュアル疾患解説　眼で見る遺伝病とターナー症候群	2	6-7	2008
戸田達史	孤発性パーキンソン病のゲノムワイドスクリーニング	ゲノム医学	8	21-26	2008
小林千浩　戸田達史	認知と遺伝子	Cognition and Dementia	7	35-43	2008
谷口真理子　戸田達史	筋ジストロフィー	小児内科	40	1308-1314	2008
水田依久子　戸田達史	孤発性パーキンソン病のメカニズム	成人病と生活習慣病	38	887-892	2008
戸田達史	Alzheimer 病と遺伝	成人病と生活習慣病	38	1205-1210	2008
戸田達史	福山型筋ジストロフィーの発見とその類縁疾患における病態	蛋白質　核酸酵素	53	1771-1780	2008
村田美穂	パーキンソン病治療薬の問題点と今後望まれる薬剤	日本病院薬剤師会雑誌	131	281-284	2008
村田美穂	パーキンソン病における併用療法のあり方と注意点	老年医学	46	365-369	2008
村田美穂	パーキンソン病薬物療法のメリット・デメリット	医学のあゆみ	225	395-399	2008
岡本智子、村田美穂	プライマリケア時代の症候の診方—振戦—	診断と治療増刊号	96	149-155	2008
村田美穂	ゾニサミドの抗パーキンソン病効果	成人病と生活習慣病	38	967-970	2008

村田美穂	パーキンソン病治療の変遷と今後の展望　薬物療法 L-dopa の効果と安全性に関する最近の知見	Prog.Med.	28	2347-2350	2008
村田美穂	パーキンソン病の治療—薬物療法の up to date—	臨床神経学	48	986-988	2008
村田美穂, 久野貞子	パーキンソン病におけるＤＢＳアンケート結果—満足度と問題点—	Pharma Medica	26(3)	6-11	2008
村田美穂	パーキンソン病	ドクターサロン	52	17-20	2008
村田美穂	パーキンソン病　最新情報	今日の健康	7	114-121	2008
村田美穂	パーキンソン病の薬物治療—最近の知見	日本医事新報	4419	105	2009
服部信孝	遺伝性パーキンソン病の遺伝子産物の機能解析から黒質神経変性のメカニズムを探る	脳21	11	372-376	2008
服部信孝, 久保紳一郎	ここまでわかったパーキンソン病(PD)の成因　遺伝性 PD の病態からわかったこと	臨床神経学	47	774-778	2008

IV. 研究成果の刊行物・別刷

Hum Genet (2008) 124:89–94
DOI 10.1007/s00439-008-0525-5

ORIGINAL INVESTIGATION

Calbindin 1, fibroblast growth factor 20, and *α-synuclein* in sporadic Parkinson's disease

Ikuko Mizuta · Tatsuhiko Tsunoda · Wataru Satake · Yuko Nakabayashi · Masahiko Watanabe · Atsushi Takeda · Kazuko Hasegawa · Kenji Nakashima · Mitsutoshi Yamamoto · Nobutaka Hattori · Miho Murata · Tatsushi Toda

Received: 4 April 2008 / Accepted: 11 June 2008 / Published online: 22 June 2008

Abstract Parkinson's disease (PD), one of the most common human neurodegenerative disorders, is characterized by the loss of dopaminergic neurons in the substantia nigra of the midbrain. Our recent case-control association study of 268 SNPs in 121 candidate genes identified *α-synuclein* (*SNCA*) as a susceptibility gene for sporadic PD ($P = 1.7 \times 10^{-11}$). We also replicated the association of *fibroblast growth factor 20* (*FGF20*) with PD ($P = 0.0089$). To find other susceptibility genes, we added 34 SNPs to the previous screen. Of 302 SNPs in a total 137 genes, but excluding *SNCA*, SNPs in *NDUFV2*, *FGF2*, *CALB1* and *B2M* showed significant association ($P < 0.01$; 882 cases and 938 control subjects). We replicated the association analysis for these SNPs in a second independent sample set (521 cases and 1,003 control subjects). One SNP, rs1805874 in *calbindin 1* (*CALB1*), showed significance in both analyses ($P = 7.1 \times 10^{-5}$; recessive model). When the analysis was stratified relative to the *SNCA* genotype, the odds ratio of *CALB1* tended to increase according to the number of protective alleles in *SNCA*. In contrast, *FGF20* was significant only in the subgroup of *SNCA* homozygote of risk allele. CALB1 is a calcium-binding protein that widely is expressed in neurons. A relative sparing of

Electronic supplementary material The online version of this article (doi:10.1007/s00439-008-0525-5) contains supplementary material, which is available to authorized users.

I. Mizuta · W. Satake · Y. Nakabayashi · T. Toda (✉)
Division of Clinical Genetics, Department of Medical Genetics, Osaka University Graduate School of Medicine, 2-2-B9 Yamadaoka, Suita, Osaka 565-0871, Japan
e-mail: toda@clgene.med.osaka-u.ac.jp

I. Mizuta · Y. Nakabayashi · T. Toda
Core Research for Evolutional Science and Technology (CREST), Japan Science and Technology Agency, Saitama 332-0012, Japan

T. Tsunoda
Laboratory for Medical Informatics, SNP Research Center, The Institute of Physical and Chemical Research (RIKEN), Yokohama, Kanagawa 230-0045, Japan

M. Watanabe
Department of Neurology, Graduate School of Comprehensive Human Sciences, University of Tsukuba, Tsukuba 305-8575, Japan

A. Takeda
Division of Neurology, Department of Neuroscience, Tohoku University Graduate School of Medicine, Sendai 980-8574, Japan

K. Hasegawa
Department of Neurology, National Hospital Organization, Sagamihara National Hospital, Sagamihara 228-8522, Japan

K. Nakashima
Department of Neurology, Tottori University Faculty of Medicine, Yonago 683-8504, Japan

M. Yamamoto
Department of Neurology, Kagawa Prefectural Central Hospital, Takamatsu 760-8557, Japan

N. Hattori
Department of Neurology, Juntendo University School of Medicine, Tokyo 113-8421, Japan

M. Murata
Department of Neurology, Musashi Hospital, National Center of Neurology and Psychiatry, Kodaira 187-8551, Japan

CALB1-positive dopaminergic neurons is observed in PD brains, compared with CALB1-negative neurons. Our genetic analysis suggests that *CALB1* is associated with PD independently of *SNCA*, and that *FGF20* is associated with PD synergistically with *SNCA*.

Introduction

Parkinson's disease (PD) (OMIM 168600), which affects one to two percent of people age 65 or older (de Rijk et al. 1997) is one of the most common human neurodegenerative diseases, second in incidence only to Alzheimer's disease (OMIM 104300). Clinical features of PD include resting tremor, bradykinesia, rigidity and postural instability. PD is characterized pathologically by the loss of dopaminergic neurons in the substantia nigra of the midbrain and by the presence of intracellular inclusions known as Lewy bodies (Shults 2006). Various types of medical management are available for PD, including drugs (L-Dopa, dopamine agonists, anti-cholinergic drugs and others) and surgery (e.g., thalamotomy, pallidotomy, deep brain stimulation) (Rascol et al. 2003). These treatments improve PD symptoms but do little to deter disease progression. Identifying risk factors for PD can thus be helpful in delaying disease onset and slowing its progression.

Genetic approaches for Mendelian-inherited PD have identified autosomal dominant genes including *α-synuclein* (*SNCA*) and *LRRK2*, as well as autosomal recessive genes *parkin*, *PINK1*, *DJ-1*, and *ATP13A2* (Thomas and Beal 2007).

However, Mendelian-inherited PD is rare compared with the far more common sporadic PD, a complex disorder caused by multiple genetic and environmental factors (Warner and Schapira 2003). Using a multiple candidate gene analysis, we previously identified and confirmed *SNCA* (4q21) as a definite susceptibility gene for sporadic PD (Mizuta et al. 2006). In addition we recently replicated the significance of *FGF20* (8p22-p21.3) (Satake et al. 2007). Here, we have found a novel PD susceptibility gene *calbindin 1* (*CALB1*, 8q21.3-q22.1) from multiple candidate gene analysis.

Methods

Subjects

We recruited two independent sample sets, comprised of individuals with Japanese ancestry. Sample Set 1, described in our previous report (Mizuta et al. 2006), included 882 unrelated sporadic PD patients (age = 64.9 ± 9.8; male/female ratio = 0.79; onset = 57.4 ± 10.9 years of age; 51 patients with a positive family history) and 938 unrelated controls without neurological disorders (age = 45.3 ± 16.3; male/female ratio = 1.10). Another independent set (Sample Set 2) consisted of 521 PD patients (age = 67.2 ± 9.7; male/female ratio = 0.87; onset = 58.8 ± 11.4 years of age; no family history) and 1,003 control subjects (106 individuals age = 58.9 ± 11.4; male/female ratio = 0.86; plus 897 age- and sex-unknown adult subjects). Diagnosis of sporadic PD was based on the presence of two or more of the cardinal features of PD (tremor, rigidity, bradykinesia, and postural instability), determined according to established criteria (Bower et al. 1999). Control subjects are healthy volunteers including spouses of patients. Informed consent was obtained from each participant, and approval for the study was obtained from the University Ethical Committees.

SNP genotyping

Genomic DNA was extracted from whole blood using FlexGene (QIAGEN). One hundred and fifteen samples treated subjected to whole genome amplification (GenomiPhi DNA Amplification Kit, GE Healthcare, Buckinghamshire, UK) were included in Sample Set 2. We genotyped the SNPs using the Invader assay (Third Wave Technologies) or TaqMan (Applied Biosystems).

Gene and SNP selection

We selected candidate genes from published reports describing genetic, pathological and biochemical findings in PD, as well as genes that participate in proposed mechanisms for PD. Finally, we included 137 genes relevant to familial PD, Lewy bodies, dopaminergic neurons, cytokines and trophic factors, mitochondrial functions, oxidative stress, proteasome function, autophagy, endoplasmic reticulum-associated degradation (ERAD) and toxins. One to seven SNPs per gene (302 SNPs total) were selected from the dbSNP and JSNP (Haga et al. 2002) databases for analysis. Of 302 SNPs in 137 genes, 268 SNPs in 121 genes had been described elsewhere (Mizuta et al. 2006).

For linkage disequilibrium (LD) analysis, information about chromosomal structure and recombination hotspots was obtained from the HapMap database (http://www.hapmap.org/) (The International HapMap Consortium 2005). Japanese tag SNPs (MAF > 0.1, $r^2 > 0.8$) were selected from the HapMap SNP pool using the ABI SNP-browser (http://www.allsnps.com/snpbrowser). Typing data for 785 control subjects were used in LD analysis.

Statistical analysis

SNPAlyze software (DYNACOM, Japan) was used for case-control study χ^2 test, haplotype analysis (Expectation-

Maximization algorithm) and pairwise LD analysis (Lewontin's coefficient D', and standardized coefficient r).

Results

This current study follows our closely related study where 268 SNPs were screened in 121 candidate genes using a case-control analysis. For the current analysis, we examined 34 additional SNPs in 17 candidate genes using a subset of Sample Set 1 (190 cases and 190 control subjects). Five SNPs of them were significant (Supplementary Table 1). Twenty-two significant SNPs from the first study and these five SNPs were then evaluated in all subjects in Sample Set 1 (882 cases and 935 control subjects). In total, this enhanced screen revealed 27 significant SNPs through genotype analysis of 302 SNPs in 137 candidate genes. (One gene, *IL1B*, was included in both the original and the enhanced screen.) Of these 27, the most significant SNP, rs7684318 in *SNCA*, had been reported previously, further confirming *SNCA* as a susceptibility gene for PD (Mizuta et al. 2006). Of the remaining 26 SNPs (Supplementary Table 2), four SNPs in *NDUFV2* (OMIM 600532), *FGF2* (OMIM 134920), *CALB1* (OMIM 114050) and *B2M* (OMIM 109700) showed *P*-values less than 0.01. They were prompted to genotyping in a second sample set (Sample Set 2) composed of 521 cases and 1,003 control subjects (Supplementary Table 2). *SNCA* rs7684318 was included in this replication study as a quality control to assure that the genotyping was consistent. After application of a Bonferroni correction for 302 SNPs ($\alpha = 1.6 \times 10^{-4}$), the association of rs1805874 in *CALB1* (8q21.3-q22.1) remained significant ($P = 7.1 \times 10^{-5}$; recessive model). The prominent association of *SNCA* rs7684318 ($P = 5.1 \times 10^{-14}$ for allele frequency) was again confirmed (Table 1).

For LD mapping, we genotyped Sample Set 1 using 10 tag SNPs selected from a 230-kb region that surrounds *CALB1* and falls between recombination hotspots (Fig. 1; Table 2). Since most of the pairwise D' values were greater than 0.9, this region is thought to be a single LD block (Fig. 1). Of the ten tag SNPs, rs1805874 and rs1805868 showed significant association with sporadic PD (Table 2). A replication study of the two SNPs using Sample Set 2 confirmed the significance of rs18058754 (Table 2). The haplotype did not show stronger association than the single SNP (Supplementary Table 3). The rs1805874-tagged SNPs are concentrated in and upstream of *CALB1*. The SNPs tagged by closely neighboring ones showing no association span outside of rs1805874-tagged SNPs. This suggests that PD-associated region is restricted in *CALB1* region (Supplementary Fig., Table 4).

Table 1 Association analysis of *CALB1* and *SNCA*

SNP (gene)	Allele (Mm)[a]		Genotype (MM/Mm/mm)		*M* frequency	*P*				HWE	
			Case	Control	Case/control	Genotype	Allele	MM + Mm versus mm	MM versus Mm + mm	Case/control	
rs1805874 (*CALB1*)	AC	Sample Set 1	549/253/32	538/319/58	0.810/0.762	0.0032	6.1×10^{-4}	0.018	0.0025	0.67/0.25	
		Sample Set 2	341/148/23	584/351/43	0.811/0.776	0.023	0.03	0.94	0.0089	0.18/0.28	
		Combined	890/401/55	1,121/670/101	0.810/0.770	3.3×10^{-4}	8.5×10^{-5}	0.1	7.1×10^{-5}	0.25/0.95	
					MM versus mm	Mm versus mm	M versus m	MM + Mm versus mm	MM versus Mm + mm		
		OR[b] (95% CI)			1.46 (1.04–2.05)	1.1 (0.77–1.56)	1.28 (1.13–1.44)	1.32 (0.95–1.85)	1.34 (1.16–1.55)		
rs7684318 (*SNCA*)	CT	Sample Set 1	385/394/89	295/472/165	0.671/0.570	2.7×10^{-9}	5.0×10^{-10}	5.7×10^{-6}	2.8×10^{-8}	0.42/0.31	
		Sample Set 2	213/226/63	323/456/185	0.649/0.572	3.1×10^{-4}	4.5×10^{-5}	0.0013	7.6×10^{-4}	0.80/0.29	
		Combined	598/620/152	618/928/350	0.663/0.571	5.5×10^{-13}	5.1×10^{-14}	8.5×10^{-10}	1.1×10^{-10}	0.65/0.96	
					MM versus mm	Mm versus mm	M versus m	MM + Mm versus mm	MM versus Mm + mm		
		OR[b] (95% CI)			2.23 (1.79–2.78)	1.54 (1.24–1.91)	1.48 (1.34–1.64)	1.81 (1.48–2.23)	1.6 (1.39–1.85)		

[a] Disease allele (M) and protective allele (m)

[b] Odds ratio (OR) was calculated in combined sample set

Table 2 Association analysis of SNPs in *CALB1* and the surrounding region

SNP	Location	Allele[a]	Genotype (11/12/22)		MAF[b]	*P*				HWE
		12	Case	Control	Case/Control	Genotype	Allele	11 + 12 versus 22	22 + 12 versus 11	Case/control
Sample Set 1										
rs1805824	*NBN* (intron)	GA	533/274/53	577/269/51	0.221/0.207	0.59	0.31	0.67	0.31	0.029/0.010
rs2097825	Intergenic	GC	236/386/221	208/416/242	0.509/0.480	0.17	0.10	0.42	0.061	0.015/0.027
rs1805860	*DECR1* (intron)	GA	431/337/89	460/338/77	0.300/0.281	0.44	0.21	0.26	0.34	0.059/0.19
rs1805868	*DECR1* (intron)	GA	448/341/63	423/378/103	0.274/0.323	0.0047	0.0015	0.0042	0.015	0.86/0.19
rs2074596	*DECR1* (intron)	GA	300/369/180	327/416/145	0.429/0.398	0.032	0.057	0.009	0.52	0.0010/0.51
rs12549239	*CALB1* (3′ flanking)	TC	76/329/461	59/348/502	0.278/0.256	0.18	0.15	0.40	0.069	0.12/0.90
rs1805874	*CALB1* (intron)	CA	32/253/549	58/319/538	0.190/0.238	0.0032	0.00061	0.0025	0.018	0.67/0.25
rs12171665	*CALB1* (5′ flanking)	GA	169/404/280	189/448/271	0.435/0.455	0.40	0.23	0.18	0.60	0.29/0.88
rs12541465		TG	617/210/15	690/185/18	0.143/0.124	0.109	0.103	0.72	0.054	0.55/0.18
rs2049815		TG	378/374/94	382/381/124	0.332/0.355	0.20	0.16	0.072	0.50	0.92/0.067
Sample Set 2										
rs1805868	*DECR1* (intron)	GA	279/189/44	468/412/83	0.271/0.300	0.077	0.092	0.99	0.031	0.14/0.57
rs1805874	*CALB1* (intron)	CA	23/148/341	43/351/583	0.189/0.224	0.023	0.030	0.0089	0.94	0.18/0.28

[a] Relative to the chromosomal orientation

[b] Minor allele frequency

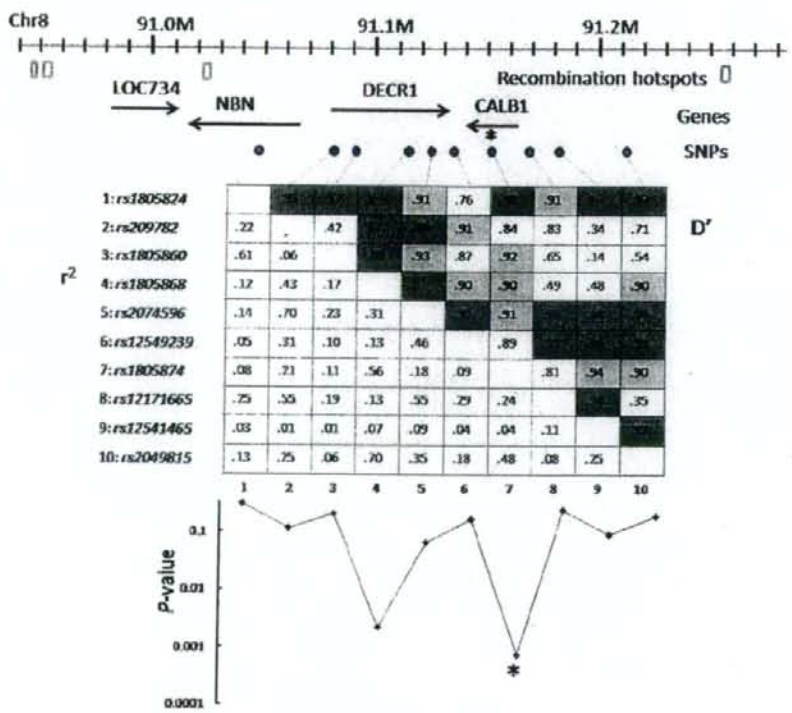

Fig. 1 LD structure and significance of association in the susceptibility region for sporadic PD. *Top* the genomic structure of the *CALB1* region, including genes (*arrows*) and recombination hotspots (*red-lined rectangles*), generated from HapMap. Ten SNPs were plotted (*closed circles*), including the originally screened rs1805874 (marked by an *asterisk*). *Middle* Pairwise *D′* (*upper right*) and r^2 (*lower left*) in 785 control subjects. *Highlighted cells* contain LD values >0.95 (*red*) or >0.9 (*pink*). *Bottom* case-control association studies in Sample Set 1 (882 cases and 938 control subjects). Log *P*-values (allele 1 vs allele 2) are plotted against the nominal location of the SNPs. The originally screened rs1805874 was indicated by an *asterisk*

Detailed association analysis in the combined sample sets (Table 1) showed the strongest association for *CALB1* rs1805874 in a recessive model ($P = 7.1 \times 10^{-5}$, OR = 1.34). The effect of *SNCA* rs7684318 (allele OR = 1.48; genotype OR = 2.23 for the CC genotype and 1.54 for CT genotype) was well described using a multiplicative model (Table 1).

Table 3 Association analysis of *CALB1* and *FGF20*, stratified by *SNCA* genotype

	Case		Control		OR (95% CI)	*P*
	CALB1 (rs1805874)					
	AA	AC + CC	AA	AC + CC		
SNCA (rs7684318)						
CC	381	205	381	227	1.11 (0.87–1.40)	0.4
CT	393	203	531	386	1.41 (1.14–1.74)	0.0017
TT	102	44	201	147	1.70 (1.12–2.56)	0.012
	FGF20 (rs1721100)					
	GG	GC + CC	GG	GC + CC		
SNCA (rs7684318)						
CC	225	360	159	448	1.76 (1.38–2.25)	5.9×10^{-6}
CT	178	429	281	629	0.93 (0.74–1.16)	0.52
TT	51	98	96	247	1.34 (0.89–2.02)	0.16

OR and *P*-values for 2 × 2 contingency table of *CALB1* and *FGF20* were calculated in *SNCA* CC, CT, and TT genotype subgroups

FGF20 rs1721100, as we reported previously, was most significant in a recessive model ($P = 0.0053$, OR = 1.24) (Satake et al. 2007). *SNCA* rs7684318 revealed the strongest effect of the three SNPs. To analyze the potential combinational effect of the three SNPs, we performed χ^2 tests stratified by *SNCA* genotypes. The OR for *CALB1* tended to increase with *SNCA* CC, CT, and TT subgroups, in this order (Table 3). In contrast, *FGF20* rs1721100 was significant in the subgroup of *SNCA* homozygote of risk allele, but not in others (Table 3).

Discussion

Numerous case-control association studies have been reported for sporadic PD candidate genes (Warner and Schapira 2003). The main development of this field includes establishment of *SNCA* and *MAPT/tau* (Zabetian et al. 2007) as susceptibility genes for PD. *SNCA* is the first identified causal gene for Mendelian-inherited PD and encodes protein of a major component of Lewy body (Polymeropoulos et al. 1997; Spillantini et al. 1997). Most of early association studies for *SNCA* focused polymorphism of Rep1, a mixed dinucleotide repeat in the promoter region (Maraganore et al. 2006). However, we previously identified prominent association in multiple SNPs tagged by rs7684318 in 3′ region of *SNCA* and reported *SNCA* as a definite susceptibility gene for sporadic PD (Mizuta et al. 2006). Although rs7684318 is rare in Caucasians, rs356165, tagged by rs7684318 in Japanese (Mizuta et al. 2006), was included in associated SNPs in German study (Mueller et al. 2005) and very recent Norwegian study (Myhre et al. 2008).

This current report extends our analysis, identifying and confirming *CALB1* as a novel susceptibility gene for this disorder. We found that *CALB1* rs1805874 was significantly associated with PD in Japanese population. The final *P*-value for the association of rs1805874 can be calculated as 2.2×10^{-5} by multiplying the *P*-values of the two independent tests ($P = 0.0025$ for sample set 1 and $P = 0.0089$ for Sample Set 2). This remains significant when Bonferroni correction was applied by multiplying the number of SNPs screened (302 SNPs) and the number of contingency tables per SNP (allele, genotype, recessive model, and dominant model) (the corrected $P = 0.027$). However, this SNP was not significant in previous genome-wide association study in Caucasians (Maraganore et al. 2005). Possible explanations of this discrepancy may include ethnicity and gene-environmental effect.

CALB1 is a 28 kDa protein containing 261 amino acids, originally described as a vitamin D-dependent Ca^{2+}-binding protein in the chick duodenum (Wasserman et al. 1968). Along with calmodulin and troponin C, CALB1 belongs to the superfamily of Ca^{2+}-binding proteins, which are characterized by the presence of an EF-hand Ca^{2+}-binding loop (Persechini et al. 1989). Though CALB1 is widely distributed in mammalian brains, it localizes within certain specific neuronal types (Jande et al. 1981). In PD, CALB1-negative dopaminergic neurons in the substantia nigra of the midbrain are lost preferentially over CALB1-positive neurons, suggesting a neuroprotective role for CALB1 (Yamada et al. 1990; Damier et al. 1999). One mechanism by which CALB1 could affect neuronal viability is through buffering excess intracellular Ca^{2+} (Chard et al. 1993). This hypothesis is supported by both in vitro (Mattson et al. 1991; McMahon et al. 1998) and in vivo (Yenari et al. 2001) experimental evidence.

It is thought that many pathways, including mitochondrial dysfunction, oxidative stress, and impairment of ubiquitin-proteasome system, underlie PD pathogenesis (Moore et al. 2005). A number of molecules are thought to participate in the pathogenic process, some of which can interact synergistically. Aggregation of SNCA protein is thought to play a crucial role in the loss of dopaminergic neurons (Goedert 2001).

Along with confirming *SNCA* and *CALB1* as susceptibility genes for PD, we recently reported replication of significant association of *FGF20* with PD (Satake et al. 2007). In our association analysis stratified by *SNCA* genotype, the OR for *CALB1* tended to increase according to the number of *SNCA* protective alleles, suggesting the possibility of a negative statistical interaction between *CALB1* and *SNCA*. In contrast, *FGF20* revealed significance only in *SNCA* CC, homozygote of disease allele, suggesting the possibility of

a synergistic statistical interaction between *FGF20* and *SNCA*. It is of interest because *FGF20* risk allele is recently reported to be correlated with high expression of SNCA (Wang et al. 2008).

Sporadic PD is a complex multigenic disorder. Combinational analysis of PD susceptibility genes is helpful to evaluate effect of each gene and to uncover pathophysiological mechanism of the disease.

Acknowledgments We are grateful to the PD patients who participated in this study. We also thank Chiyomi Ito, Satoko Suzuki, and Dr. Yoshio Momose for help in performing the study; Drs. Akira Oka, Hidetoshi Inoko, and Katsushi Tokunaga for control samples; and Dr. Jennifer Logan for editing the manuscript. This work was supported by a grant from Core Research for Evolutional Science and Technology (CREST), Japan Science and Technology Agency (JST); by the twenty-first Century COE program and KAKENHI (17019044 and 19590990), both from the Ministry of Education, Culture, Sports, Science, and Technology of Japan; and by the Grant-in-Aid for "the Research Committee for the Neurodegenerative Diseases" of the Research on Measures for Intractable Diseases and Research Grant (H19-Genome-Ippan-001), all from the Ministry of Health, Labor, and Welfare of Japan.

References

Bower JH, Maraganore DM, McDonnell SK, Rocca WA (1999) Incidence and distribution of parkinsonism in Olmsted County, Minnesota, 1976–1990. Neurology 52:1214–1220

Chard PS, Bleakman D, Christakos S et al (1993) Calcium buffering properties of calbindin D28k and parvalbumin in rat sensory neurones. J Physiol 472:341–357

Damier P, Hirsch EC, Agid Y, Graybiel AM (1999) The substantia nigra of the human brain II. Patterns of loss of dopamine-containing neurons in Parkinson's disease patterns of loss of dopamine-containing neurons in Parkinson's disease. Brain 122:1437–1448

de Rijk MC, Tzourio C, Breteler MMB et al (1997) Prevalence of parkinsonism and Parkinson's disease in Europe: the EUROPARKINSON collaborative study. J Neurol Neurosurg Psychiatry 62:10–15

Goedert M (2001) Alpha-synuclein and neurodegenerative diseases. Nat Rev Neurosci 2:492–501

Haga H, Yamada R, Ohnishi Y et al (2002) Gene-based SNP discovery as part of the Japanese Millennium Genome Project: identification of 190562 genetic variations in the human genome. J Hum Genet 47:605–610

Jande SS, Maler L, Lawson DEM (1981) Immunohistochemical mapping of vitamin D-dependent calcium-binding protein in brain. Nature 294:765–767

Maraganore DM, de Andrade M, Lesnick TG et al (2005) High-resolution whole-genome association study of Parkinson disease. Am J Hum Genet 77:685–693

Maraganore DM, de Andrade M, Elbaz A et al (2006) Collaborative analysis of α-synuclein gene promoter variability and Parkinson disease. JAMA 296:661–670

Mattson MP, Rychlik B, Chu C, Christakos S (1991) Evidence for calcium-reducing and excito-protective roles for the calcium-binding protein calbindin-D_{28K} in cultured hippocampal neurons. Neuron 6:41–51

McMahon A, Wong BS, Iacopino AM et al (1998) Calbindin-D_{28K} buffers intracellular calcium and promotes resistance to degeneration in PC12 cells. Mol Brain Res 54:56–63

Mizuta I, Satake W, Nakabayashi Y et al (2006) Multiple candidate gene analysis identifies *α-synuclein* as a susceptibility gene for sporadic Parkinson's disease. Hum Mol Genet 15:1151–1158

Moore DJ, West AB, Dawson VL, Dawson TM (2005) Molecular pathophysiology of Parkinson's disease. Annu Rev Neurosci 28:57–87

Mueller JC, Fuchs J, Hofer A et al (2005) Multiple regions of α-synuclein are associated with Parkinson's disease. Ann Neurol 57:535–541

Myhre R, Toft M, Kachergus J, Hulihan MM, Aasly JO, Klungland H, Farrer MJ (2008) Multiple *alpha-synuclein* gene polymorphisms are associated with Parkinson's disease in a Norwegian population. Acta Neurol Scand (in press)

Persechini A, Moncrief ND, Kretsinger RH (1989) The EF-hand family of calcium-modulated proteins. Trends Neurosci 12:462–467

Polymeropoulos MH, Lavedan C, Leroy E et al (1997) Mutation in the α-synuclein gene identified in families with Parkinson's disease. Science 276:2045–2047

Rascol O, Payoux P, Ory F et al (2003) Limitations of current Parkinson's disease therapy. Ann Neurol 53(Suppl 3):S3–S12

Satake W, Mizuta I, Suzuki S et al (2007) Fibroblast growth factor 20 gene and Parkinson's disease in the Japanese population. Neuroreport 18:937–940

Shults CW (2006) Lewy bodies. Proc Natl Acad Sci USA 103:1661–1668

Spillantini MG, Schmidt ML, Lee VM-Y et al (1997) α-Synuclein in Lewy bodies. Nature 388:839–840

The International HapMap Consortium (2005) A haplotype map of the human genome. Nature 437:1299–1320

Thomas B, Beal MF (2007) Parkinson's disease. Hum Mol Genet 16:R183–R194

Wang G, van der Walt JM, Mayhew G et al (2008) Variation in the miRNA-433 binding site of FGF20 confers risk for Parkinson disease by overexpression of α-synuclein. Am J Hum Genet 82:283–289

Warner TT, Schapira AH (2003) Genetic and environmental factors in the cause of Parkinson's disease. Ann Neurol 53(Suppl 3):S16–S23

Wasserman RH, Corradino RA, Taylor AN (1968) Vitamin D-dependent calcium-binding protein. Purification and some properties. J Biol Chem 243:3978–3986

Yamada T, McGeer PL, Baimbridge KG, McGeer EG (1990) Relative sparing in Parkinson's disease of substantia nigra dopamine neurons containing calbindin-D_{28K}. Brain Res 526:303–307

Yenari MA, Minami M, Sun GH et al (2001) Calbindin D28K overexpression protects striatal neurons from transient focal cerebral ischemia. Stroke 32:1028–1035

Zabetian CP, Hutter CM, Factor SA et al (2007) Association analysis of *MAPT H1* haplotype and subhaplotypes in Parkinson's disease. Ann Neurol 62:137–144

VOLUME 11 NUMBER 8 AUGUST 2008
www.nature.com/natureneuroscience

nature neuroscience

Pikachurin at the ribbon synapse

Task difficulty modulates attentional effects in V1

Hypoxia causes axon guidance deficits

nature neuroscience

Pikachurin, a dystroglycan ligand, is essential for photoreceptor ribbon synapse formation

Shigeru Sato[1–3], Yoshihiro Omori[1], Kimiko Katoh[1], Mineo Kondo[4], Motoi Kanagawa[5], Kentaro Miyata[4], Kazuo Funabiki[6], Toshiyuki Koyasu[4], Naoko Kajimura[7], Tomomitsu Miyoshi[8], Hajime Sawai[8], Kazuhiro Kobayashi[5], Akiko Tani[1], Tatsushi Toda[5], Jiro Usukura[9], Yasuo Tano[2], Takashi Fujikado[2,3] & Takahisa Furukawa[1]

Exquisitely precise synapse formation is crucial for the mammalian CNS to function correctly. Retinal photoreceptors transfer information to bipolar and horizontal cells at a specialized synapse, the ribbon synapse. We identified pikachurin, an extracellular matrix–like retinal protein, and observed that it localized to the synaptic cleft in the photoreceptor ribbon synapse. *Pikachurin* null-mutant mice showed improper apposition of the bipolar cell dendritic tips to the photoreceptor ribbon synapses, resulting in alterations in synaptic signal transmission and visual function. Pikachurin colocalized with both dystrophin and dystroglycan at the ribbon synapses. Furthermore, we observed direct biochemical interactions between pikachurin and dystroglycan. Together, our results identify pikachurin as a dystroglycan-interacting protein and demonstrate that it has an essential role in the precise interactions between the photoreceptor ribbon synapse and the bipolar dendrites. This may also advance our understanding of the molecular mechanisms underlying the retinal electrophysiological abnormalities observed in muscular dystrophy patients.

The establishment of precise synaptic connections between neurons in the developing and mature CNS is crucial for normal nervous system functions, including perception, memory and cognition. Thus, elucidating the mechanisms by which synapses develop and are modified is a central aim in neurobiology. Over the past few decades, a large number of protein components have been identified that are required for synapse morphogenesis and neurotransmitter release[1,2]. However, the molecules and mechanisms underlying specific synapse connections in the vertebrate CNS are still poorly understood.

The neural retina is developmentally a part of the CNS and is where the first stage of visual signal processing occurs. Visual information is transmitted from photoreceptor cells to the ganglion cells via bipolar interneurons. The photoreceptor axon terminal forms a specialized structure, the ribbon synapse, which specifically connects photoreceptor synaptic terminals with bipolar and horizontal cell terminals in the outer plexiform layer (OPL) of the retina. Although various presynaptic factors that are required for synaptic ribbon structure, such as CtBp2/RIBEYE, piccolo and bassoon, have been identified[3,4], the mechanism of ribbon synapse apposition specific to bipolar and horizontal terminals remains totally unknown.

Mutations in the dystrophin-glycoprotein complex (DGC) cause various forms of muscular dystrophy[5]. Dystroglycan, a central component of the DGC, functions as a cellular receptor that is expressed in a variety of tissues, including the CNS[6]. Dystroglycan precursor protein is cleaved into two subunits, α-dystroglycan and β-dystroglycan[7]. α-dystroglycan is a heavily glycosylated extracellular protein and has the potential to bind to several extracellular proteins containing the laminin-G domain, including laminin-α1, laminin-α2, agrin, perlecan and neurexins[8–11]. The DGC components are also expressed in the retina[12–15]. Altered electroretinograms (ERGs) are frequently found in individuals with Duchenne and Becker muscular dystrophy, indicating that the DGC is necessary for normal retinal physiology[16–18]. However, the functional role of DGC in the retina is elusive.

We isolated and characterized mouse pikachurin, a dystroglycan ligand in the retina. To the best of our knowledge, pikachurin is the first dystroglycan ligand to interact with the presynaptic dystroglycan. Our results demonstrate that pikachurin is critically involved in both the normal photoreceptor ribbon synapse formation and physiological functions of visual perception. This may also shed light on the molecular mechanisms underlying the retinal

[1]Department of Developmental Biology, Osaka Bioscience Institute, 6-2-4 Furuedai, Suita, Osaka, 565-0874, Japan. [2]Department of Ophthalmology, Osaka University Graduate School of Medicine, 2-2 Yamadaoka, Suita, Osaka, 565-0871, Japan. [3]Department of Visual Science, Osaka University Graduate School of Medicine, 2-2 Yamadaoka, Suita, Osaka, 565-0871, Japan. [4]Department of Ophthalmology, Nagoya University Graduate School of Medicine, 65 Tsuruma-cho, Showa-ku, Nagoya, 466-8550, Japan. [5]Division of Clinical Genetics, Department of Medical Genetics, Osaka University Graduate School of Medicine, 2-2 Yamadaoka, Suita, Osaka, 565-0871, Japan. [6]Department of Systems Biology, Osaka Bioscience Institute, 6-2-4 Furuedai, Suita, Osaka, 565-0874, Japan. [7]Research Center for Ultrahigh-Voltage Electron Microscopy, Osaka University, 7-1 Mihogaoka, Ibaraki, Osaka, 567-0047, Japan. [8]Department of Physiology, Osaka University Graduate School of Medicine, 2-2 Yamadaoka, Suita, Osaka, 565-0871, Japan. [9]Department of Materials Physics and Engineering, Nagoya University Graduate School of Engineering, 1-1 Furo-cho, Chikusa-ku, Nagoya, 464-8603, Japan. Correspondence should be addressed to T.F. (furukawa@obi.or.jp).

Received 1 May; accepted 12 June; published online 20 July 2008; doi:10.1038/nn.2160

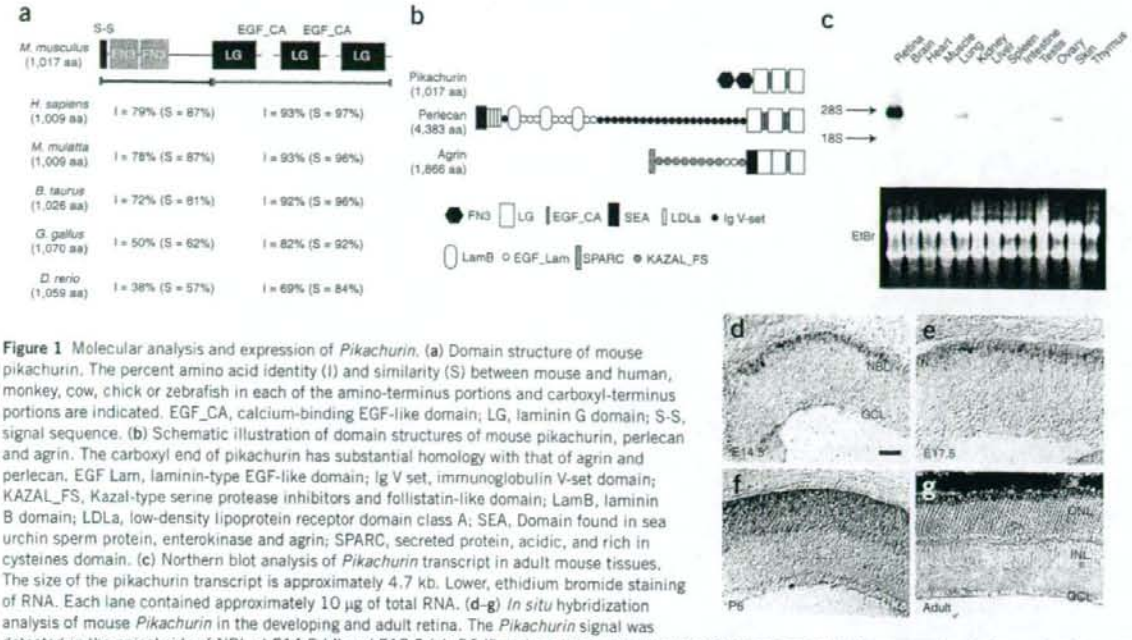

Figure 1 Molecular analysis and expression of *Pikachurin*. (**a**) Domain structure of mouse pikachurin. The percent amino acid identity (I) and similarity (S) between mouse and human, monkey, cow, chick or zebrafish in each of the amino-terminus portions and carboxyl-terminus portions are indicated. EGF_CA, calcium-binding EGF-like domain; LG, laminin G domain; S-S, signal sequence. (**b**) Schematic illustration of domain structures of mouse pikachurin, perlecan and agrin. The carboxyl end of pikachurin has substantial homology with that of agrin and perlecan. EGF Lam, laminin-type EGF-like domain; Ig V set, immunoglobulin V-set domain; KAZAL_FS, Kazal-type serine protease inhibitors and follistatin-like domain; LamB, laminin B domain; LDLa, low-density lipoprotein receptor domain class A; SEA, Domain found in sea urchin sperm protein, enterokinase and agrin; SPARC, secreted protein, acidic, and rich in cysteines domain. (**c**) Northern blot analysis of *Pikachurin* transcript in adult mouse tissues. The size of the pikachurin transcript is approximately 4.7 kb. Lower, ethidium bromide staining of RNA. Each lane contained approximately 10 μg of total RNA. (**d–g**) *In situ* hybridization analysis of mouse *Pikachurin* in the developing and adult retina. The *Pikachurin* signal was detected in the apical side of NBL at E14.5 (**d**) and E17.5 (**e**). P6 (**f**) and adult (**g**) retina had the *Pikachurin* signal in the prospective photoreceptor layer and the photoreceptor layer, respectively. GCL, ganglion cell layer; INL, inner nuclear layer; ONL, outer nuclear layer. Scale bar represents 50 μm.

electrophysiological abnormalities observed in individuals with Duchenne and Becker muscular dystrophy.

RESULTS

Isolation of pikachurin

Otx2 is an important transcription factor for the cell fate determination and development of retinal photoreceptor cells[19,20]. We previously reported that the cell fates of both rod and cone photoreceptors are converted to that of amacrine-like cells in the *Otx2* conditional knockout (CKO) mouse line that was created by mating $Otx2^{flox/flox}$ mice with *Crx-Cre* transgenic mice, which express cre recombinase in developing photoreceptors. We hypothesized that transcripts from various genes, which are important for photoreceptor development, maintenance and function, are relatively downregulated in the *Otx2* CKO retina compared with those of the wild-type retina. To identify genes that regulate photoreceptor development, we carried out a microarray analysis comparing the retinal gene expression profiles of wild-type and *Otx2* CKO mouse retinas (data not shown). In this screen, we identified *Pikachurin*, a gene that encoded a previously unknown extracellular matrix (ECM)-like protein containing laminin G and EGF-like domains (**Fig. 1a**).

To confirm whether or not *Pikachurin* transcription is regulated by Otx2, we carried out an RT-PCR analysis. *Pikachurin* expression was absent in the *Otx2* CKO mice retina (**Supplementary Fig. 1** online), indicating that *Pikachurin* is actually regulated by Otx2. We isolated a full-length cDNA and found that *Pikachurin* encodes a 1,017 amino acid protein that contains an N-terminal signal sequence, two fibronectin 3 (FN3), three laminin G and two EGF-like domains (**Fig. 1a** and **Supplementary Fig. 1**). We found that pikachurin was highly conserved in vertebrates, as indicated by the sequence similarity between mouse and zebrafish in the N-terminal FN3-containing domain (57%) and in the C-terminal laminin G repeats (84%) (**Fig. 1a** and **Supplementary Fig. 1**). The C-terminal half of pikachurin showed substantial similarity with agrin and perlecan (**Fig. 1b**).

Pikachurin is expressed in developing photoreceptors

To examine the tissue specificity of *Pikachurin* expression, we carried out a northern blot analysis with adult mouse tissues. We observed a single, strong 4.7-kb band in the mouse retina and faint bands in the lung and ovary (**Fig. 1c**). Although the *Pikachurin* transcript was not detected in the brain by northern blot analysis, we observed a faint *Pikachurin* band by RT-PCR analysis (**Supplementary Fig. 1**). We also detected *Pikachurin* expression in the pineal gland by RT-PCR but not in the inner ear at adult stage (**Supplementary Fig. 1**).

Furthermore, we carried out *in situ* hybridization using developing and adult mouse eye sections (**Fig. 1d–g**). *Pikachurin* expression was first detected at embryonic day 14.5 (E14.5) in the outer part of the neuroblastic layer (NBL), corresponding to the prospective photoreceptor layer (**Fig. 1d**). At this stage, cone genesis has reached its peak period and rod generation has been initiated[21]. At E17.5, a steady signal was observed (**Fig. 1e**). During postnatal retinal development, *Pikachurin* expression was observed in the photoreceptor layer (**Fig. 1f**) at postnatal day 6 (P6). This decrease in pikachurin expression in the later stages of photoreceptor development was confirmed by northern blotting (**Supplementary Fig. 1**). The expression level of pikachurin peaked at P6 and then decreased after this time point; however, a detectable level of pikachurin expression was maintained in the adult retina (**Fig. 1g**).

Pikachurin localizes in the vicinity of synaptic ribbon

To investigate the localization of pikachurin protein, we raised an antibody to pikachurin. We immunostained sections of adult mouse retina using this antibody. In the adult retina, pikachurin specifically localized to the OPL (**Fig. 2a**) in a punctate pattern (**Fig. 2b**). In

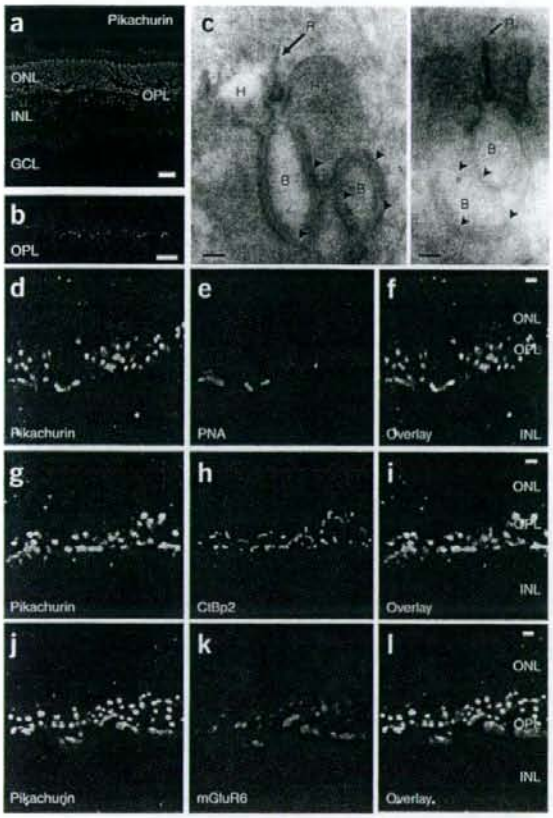

Figure 2 Pikachurin localizes to the synaptic cleft of photoreceptor ribbon synapse in the OPL. (**a**,**b**) Immunostaining of 6-month-old wild-type retina using antibody to pikachurin (red) with DAPI (blue) (**a**), which stains nuclei, or without DAPI at a higher magnification (**b**). Pikachurin localized to the OPL in the adult mouse retina in punctated pattern. Scale bars represent 20 μm in **a** and 10 μm in **b**. (**c**) Ultrastructural analysis of pikachurin localization in the ribbon synapse by electron microscopic immunocytochemistry. The pikachurin signals were localized to the synaptic cleft in the rod spherule (arrow heads). B and H indicate synaptic terminals of bipolar and horizontal cells, respectively. R indicates a synaptic ribbon. Scale bar represents 100 nm. (**d**–**f**) Confocal images of OPLs that were double-labeled with antibody to pikachurin (green) and PNA (red), a marker for cone pedicles of synaptic terminals, showing that pikachurin was colocalized with cone synaptic terminus. (**g**–**i**) Pikachurin-positive (green) puncta were localized to the INL side of horseshoe-like structures of synaptic ribbons that stained with CtBp2 (red), indicating that pikachurin is juxtaposed to, but not overlapping with, the synaptic ribbon structure. (**j**–**l**) Pikachurin (green) signal was observed at the photoreceptor side of mGluR6 staining (red), which is restricted to the postsynaptic site of the ON bipolar cells in the ribbon synapse of OPL. GCL, ganglion cell layer; INL, inner nuclear layer; ONL, outer nuclear layer, OPL, outer plexiform layer. Scale bars represent 20 μm in **d**–**l**.

contrast, no pikachurin signal was detected in the inner plexiform layer (IPL), where ribbon synapses are formed between bipolar cells and either ganglion or amacrine cells (data not shown).

To investigate more precisely the localization of pikachurin in the OPL, we carried out electron microscopic immunocytochemistry using our antibody to pikachurin. As shown in **Figure 2c**, the terminus of rod photoreceptors usually contains a single large ribbon that bends around four deeply invaginating postsynaptic elements, the dendrites of bipolar cells and processes of horizontal cells[3]. The pikachurin signals were mainly observed in the synaptic cleft around the bipolar cell dendritic tips in the rod spherule (**Fig. 2c**).

To examine whether pikachurin localizes to the cone pedicle, we immunostained the retina using our antibody to pikachurin and rhodamine-labeled peanut agglutinin (PNA), which specifically binds to glycolipids on the surface of cone pedicles[22]. PNA signals overlapped with those of pikachurin, indicating that pikachurin localized to cone synaptic terminals as well as to rod synaptic terminals (**Fig. 2d–f**).

Next, we analyzed the localization of pikachurin by staining with the synaptic ribbon markers bassoon and CtBp2/RIBEYE. Bassoon is a presynaptic cytomatrix protein that is essential for photoreceptor ribbon synapse formation and localizes to the base of the photoreceptor synaptic ribbon, a site of neurotransmitter release[23]. CtBp2/RIBEYE is a specific component of synaptic ribbons in the OPL and IPL of the retina[24]. We observed that pikachurin localized in the ribbon synapses to the inner nuclear–layer side of horseshoe-like structures of synaptic ribbons stained with bassoon (data not shown) and CtBp2/RIBEYE (**Fig. 2g–i**).

The localization of metabotropic glutamate receptor subtype 6 (mGluR6) is restricted to the postsynaptic site of ON bipolar cells in the ribbon synapses of the OPL[25]. We observed the pikachurin signal at the photoreceptor side of mGluR6 staining with a small partial overlap (**Fig. 2j–l**). These results suggest that pikachurin localizes to the synaptic cleft of the ribbon synapse primarily around the postsynaptic terminals of bipolar cells.

Pikachurin is required for apposition of bipolar dendrite

To investigate a possible role for *Pikachurin* in ribbon synapse formation and/or maintenance of the retina, we generated *Pikachurin* null mice by targeted gene disruption. We deleted the first exon, which contains a start codon, of the pikachurin open reading frame (**Fig. 3a**). We confirmed the deletion in the genomic DNA of the *Pikachurin* null mouse by Southern blot (**Fig. 3b**). Total RNAs from the adult retina were analyzed by northern blots using 5′ and 3′ fragments of mouse *Pikachurin* cDNA as probes. No substantial *Pikachurin* transcript or protein was detected in *Pikachurin* null mouse retinas (**Fig. 3c,d** and **Supplementary Fig. 2** online).

Pikachurin$^{-/-}$ mice were born in Mendelian ratios (data not shown). Both *Pikachurin*$^{+/-}$ and *Pikachurin*$^{-/-}$ mice showed no gross morphological abnormalities, and were viable and fertile under normal conditions in the animal facility. Histological examination revealed no obvious differences among wild-type, *Pikachurin*$^{+/-}$ and *Pikachurin*$^{-/-}$ mouse retinas at 6 months (**Fig. 3e–m** and **Supplementary Fig. 3** online).

To examine ultrastructural differences between wild-type and *Pikachurin*$^{-/-}$ mouse retinas, we carried out a conventional electron microscopy analysis. Although we did not find any substantial difference in the photoreceptor outer segments and ribbon synapses in the IPL (data not shown), we observed an absence of the tips of the bipolar cell dendrites in the *Pikachurin*$^{-/-}$ rod ribbon synapses (**Fig. 4a–d**) as well as those of cone photoreceptors (**Supplementary Fig. 4** online). To further examine this result, we analyzed the photoreceptor synaptic terminals of the wild-type and *Pikachurin*$^{-/-}$ retinas quantitatively (**Fig. 4e**). We prepared ultrathin sections from adult (3 month old) wild-type and *Pikachurin*$^{-/-}$ mouse retinas and randomly photographed them. For the quantitative analysis, we focused on rod photoreceptors, as they comprise ~99% of the photoreceptors in the

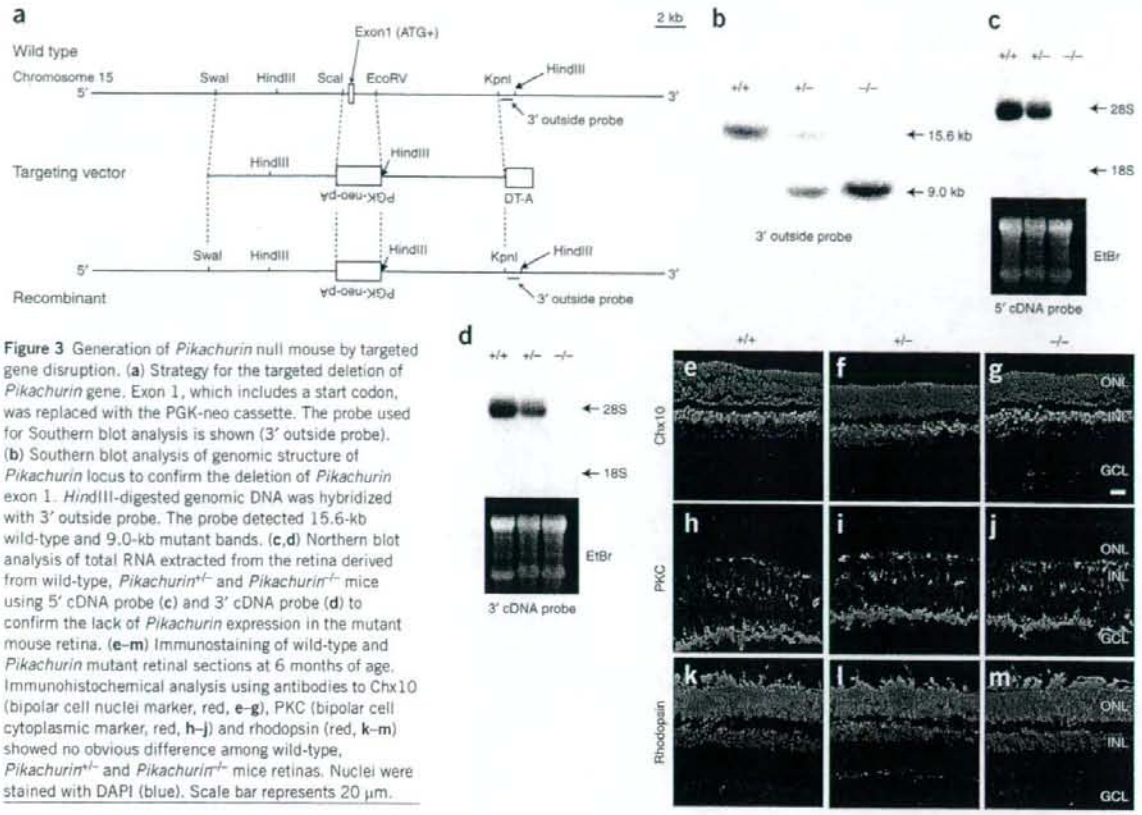

Figure 3 Generation of *Pikachurin* null mouse by targeted gene disruption. (**a**) Strategy for the targeted deletion of *Pikachurin* gene. Exon 1, which includes a start codon, was replaced with the PGK-neo cassette. The probe used for Southern blot analysis is shown (3′ outside probe). (**b**) Southern blot analysis of genomic structure of *Pikachurin* locus to confirm the deletion of *Pikachurin* exon 1. *Hin*dIII-digested genomic DNA was hybridized with 3′ outside probe. The probe detected 15.6-kb wild-type and 9.0-kb mutant bands. (**c**,**d**) Northern blot analysis of total RNA extracted from the retina derived from wild-type, *Pikachurin*$^{+/-}$ and *Pikachurin*$^{-/-}$ mice using 5′ cDNA probe (**c**) and 3′ cDNA probe (**d**) to confirm the lack of *Pikachurin* expression in the mutant mouse retina. (**e**–**m**) Immunostaining of wild-type and *Pikachurin* mutant retinal sections at 6 months of age. Immunohistochemical analysis using antibodies to Chx10 (bipolar cell nuclei marker, red, **e**–**g**), PKC (bipolar cell cytoplasmic marker, red, **h**–**j**) and rhodopsin (red, **k**–**m**) showed no obvious difference among wild-type, *Pikachurin*$^{+/-}$ and *Pikachurin*$^{-/-}$ mice retinas. Nuclei were stained with DAPI (blue). Scale bar represents 20 μm.

mouse retina[23]. A normal rod synaptic terminus contains a single ribbon synaptic site, where glutamate is released onto the postsynaptic elements, horizontal cell processes and rod bipolar cell dendrites. The postsynaptic elements invaginate into the rod terminal and form a triadic or tetradic configuration adjacent to the ribbon site (**Fig. 4a** and **Supplementary Fig. 5** online)[23,26]. In the adult *Pikachurin*$^{-/-}$ retina, we observed rod terminals containing invaginated bipolar terminals in only 3% of the sections, whereas we detected bipolar terminals in 53% of the wild-type retina (χ^2 test; $P < 0.001$; **Fig. 4e**). We used ultrathin sections; the vertical alignment of the sections was confirmed using photoreceptor outer segments as markers (**Fig. 4c**,**d**). We also found that the morphology of rod synaptic terminals varied widely even in the wild-type retina. Therefore, to confirm the precise structure of abnormal ribbon synapses in the adult *Pikachurin*$^{-/-}$ retina, we carried out electron tomography by ultrahigh-voltage electron microscopy (**Fig. 4f**–**k** and **Supplementary Movies 1**–**6**). We collected images from −60° to +60° at 2° intervals around a single axis from adult (3 month old) wild-type and *Pikachurin*$^{-/-}$ mouse retinas. The electron tomography indicates that in the terminals of bipolar cells do not appose to the synaptic terminals in the rod photoreceptor ribbon synapses the adult *Pikachurin*$^{-/-}$ retina (**Fig. 4j**,**k**).

We observed that the bipolar dendritic tips did not enter the invaginations in photoreceptor synaptic terminals in the *Pikachurin*$^{-/-}$ mice, but where do they end up? To address this question, we co-immunostained ribbon synapses using several synaptic markers. In the *Pikachurin*$^{-/-}$ mice, the bipolar cells, stained with protein kinase C (PKC; **Fig. 4l**,**m**), developed dendrites to the outer plexiform layer as well as they did in the wild type. mGluR6 accumulated at the tip of bipolar cell dendrites in both the wild-type and *Pikachurin*$^{-/-}$ mouse retina (**Fig. 4l**,**m**). CtBP2 was observed in the vicinity of the tips of bipolar dendrites in both the wild-type and *Pikachurin*$^{-/-}$ retina (**Fig. 4n**,**o**). A similar distribution of cone synaptic marker, PNA, was also observed in cone photoreceptor terminals (**Fig. 4p**,**q**). These data suggest that the bipolar dendritic terminals remain in close vicinity to photoreceptor terminals and seem to retain at least some integrity for the connection between photoreceptors and bipolar cells, even in the *Pikachurin*$^{-/-}$ retina.

Pikachurin is required for synaptic signal transmission

To evaluate the physiological function of *Pikachurin in vivo*, we measured ERGs on 2-month-old wild-type and *Pikachurin*$^{-/-}$ mice (**Fig. 5a**–**f**). The scotopic ERGs elicited by different stimulus intensities from a wild-type and a *Pikachurin*$^{-/-}$ mice are shown in **Figure 5a**. In the wild-type mouse, only a positive b-wave, which originates from the rod bipolar cells[27], was seen at lower stimulus intensities (−5.0 to −3.0 log cd s m^{-2}). At higher stimulus intensities (−1.0 to 1.0 log cd s m^{-2}), the negative a-wave, which originates mainly from the activity of the rod photoreceptors, appeared. The amplitude and implicit time of the a-wave of the dark-adapted ERGs were nearly the same for both types of mice, indicating that the rod photoreceptors are functioning normally in *Pikachurin*$^{-/-}$ mice (**Fig. 5a**). In contrast, the amplitude of the dark-adapted ERG b-wave in *Pikachurin*$^{-/-}$ mice

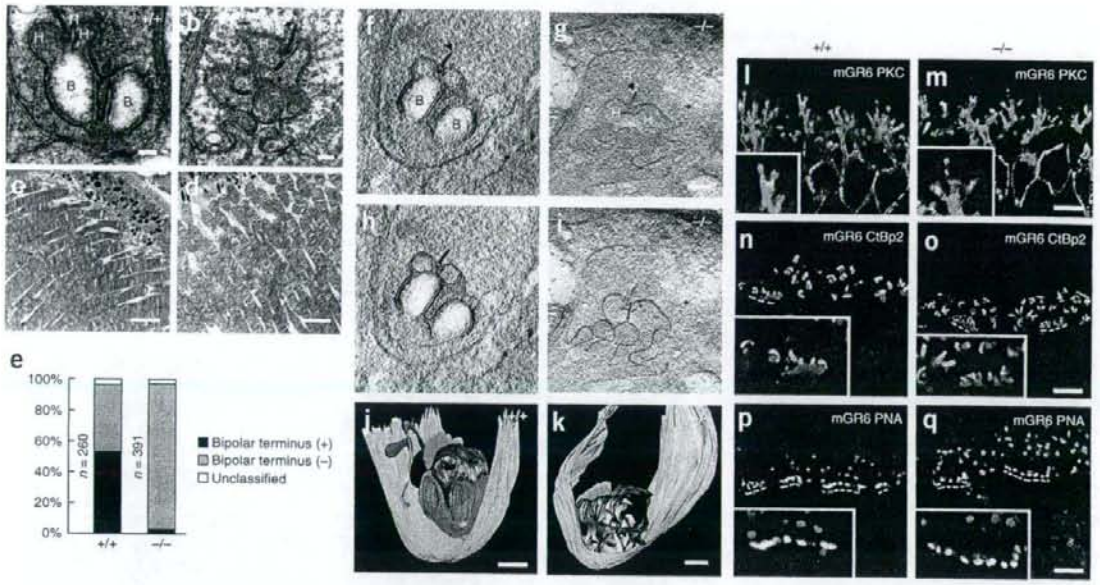

Figure 4 Pikachurin is required for proper apposition of bipolar dendritic tips to the photoreceptor synaptic terminus. (**a–d**) Ultrastructural analysis of ribbon synapses (**a**,**b**) and outer segments (**c**,**d**) in wild-type (**a**,**c**) and *Pikachurin*$^{-/-}$ (**b**,**d**) mouse retinas. Synaptic ribbon (R), horizontal cell processes (H) and bipolar cell dendrites (B) are shown. Scale bars represent 200 nm in **a** and **b** and 5 μm in **c** and **d**. (**e**) Quantitative analysis of defective bipolar cell dendrites in the wild-type (+/+) and *Pikachurin*$^{-/-}$ mouse retina. (**f–k**) Electron tomography of rod photoreceptor synapse terminals using ultrahigh-voltage electron microscopy. Representative images of retinal sections derived from wild-type (**f**,**h**,**j**) and *Pikachurin*$^{-/-}$ retinas (**g**,**i**,**k**). Representative demarcation of bipolar dendritic tips (magenta), horizontal processes (dark blue), ribbon (green) and rod plasma membrane (light blue) for tomography are shown for wild-type (**h**) and *Pikachurin*$^{-/-}$ (**i**) retinas (see **Supplementary Movies 1–6**). Scale bar = 300 nm. (**l–q**) Bipolar cell dendrites ended in the vicinity of photoreceptor terminals in *Pikachurin*$^{-/-}$ retina. mGluR6 (red) localized to the tip of bipolar cell dendrites stained with antibody to PKC (green) both in wild-type (**l**) and *Pikachurin*$^{-/-}$ retinas (**m**). The tips of bipolar cell dendrites stained with antibody to mGluR6 (red) localized in the vicinity of photoreceptor synaptic ribbons (green) both in the wild-type (**n**) and *Pikachurin*$^{-/-}$ retinas (**o**). Clustered cone synaptic terminals (broken lines) stained with PNA (green) colocalized with the tips of bipolar cell dendrites (red) in the wild-type (**p**) and the *Pikachurin*$^{-/-}$ (**q**) retinas.

was reduced at lower stimulus intensities of –5.0 to –3.0 log cd s m^{-2} but approached the normal range at higher stimulus intensities of –1.0 to 1.0 log cd s m^{-2} (**Fig. 5b**).

The most notable finding in this mutant mouse was the delay in the scotopic ERG b-wave (**Fig. 5c**). The implicit times of the scotopic ERG b-wave were severely delayed at all stimulus intensities, and the delay was more than 100 ms at the highest intensities. These results suggest that the signal transmission from the rod photoreceptors to the rod bipolar cells is less sensitive and is delayed in this mutant mouse.

To determine whether the abnormality in the signal transmission from the photoreceptors to the bipolar cells exists in the cone pathway, we recorded photopic ERGs from both types of mice (**Fig. 5d**). The amplitude of the a-wave of the photopic ERGs in *Pikachurin*$^{-/-}$ mouse was relatively larger than that of wild-type mouse, which was a result of the delay and reduction of the positive b-wave (**Fig. 5d**). The amplitude of the b-wave of the photopic ERGs was reduced and the implicit times were delayed at all stimulus intensities (**Fig. 5e**,**f**). These results indicate that the signal transmission from cone photoreceptors to the cone bipolar cells was also impaired in the *Pikachurin*$^{-/-}$ mouse.

We also recorded the collicular visual-evoked potentials (VEPs) in the *Pikachurin*$^{-/-}$ mouse. We did not observe any differences in the VEPs of wild-type and *Pikachurin*$^{-/-}$ mice in both scotopic and photopic conditions (**Fig. 5g**,**h**). This result suggests that VEPs may not be sensitive enough to reflect the ERG b-wave delay that we observed in the mutant retina and that the visual transmission pathway in the brain is not affected in *Pikachurin*$^{-/-}$ mice. We then investigated the optokinetic responses (OKRs) of 3-month-old wild-type and *Pikachurin*$^{-/-}$ mice induced by rotation of a screen with various spatial frequencies of black and white stripes (**Fig. 5i–k**). The *Pikachurin*$^{-/-}$ mouse showed similar OKRs by rotation of screens with 15- and 1.92-deg frequencies (gain was close to 1.0; **Fig. 5j**,**k**); however, its OKR at the 1.25-deg screen was significantly weaker than that of wild-type mice (unpaired *t* test, $P < 0.01$; **Fig. 5j**,**k**). Rotation of the 0.91-deg screen did not show significant OKR difference in either line ($P = 0.20$; **Fig. 5j**,**k**). Thus, *Pikachurin*$^{-/-}$ mice did not show noticeable impairment with relatively large angle stripes, but their sensitivity to small angle stripes was significantly impaired.

Pikachurin is a physiological ligand of α-dystroglycan

Many individuals with Duchenne muscular dystrophy (DMD) and Becker muscular dystrophy (BMD) have been known to show an abnormal dark-adapted ERG b-wave[17,28,29]. In mice, previous reports showed that certain dystrophin-disrupted alleles (*mdx*^{Cv2} and *mdx*^{Cv4}, alleles of *Dmd*) caused prolongation of the implicit time of the b-wave[18]. Functional defects of α-dystroglycan in *Large*-deficient mice (*Large*^{myd} and *Large*^{vls}) also produce a similar ERG phenotype to *Pikachurin* null mice[30]. In addition, agrin, perlecan and several laminin α-isoforms can all interact with α-dystroglycan by a laminin G domain–dependent mechanism[9]. These observations suggest that there is a possible functional interaction between dystroglycan and pikachurin. To investigate this issue, we first examined the localization of pikachurin, dystroglycan and dystrophin by co-immunostaining in

the retina (**Fig. 6a–f**). At 6 months, pikachurin stained in a grainy pattern in the OPL of the retina (**Fig. 6a,d**). Notably, both β-dystroglycan and dystrophin were expressed in a similar grainy pattern, overlapping with pikachurin signals (**Fig. 6b,c,e,f**).

As shown above (**Fig. 1a,b**), structural anticipation suggests that pikachurin LG domains have similarity with LG domains of agrin and perlecan. Because both proteins are known to bind to α-dystroglycan via their LG domains[10,31], we investigated whether pikachurin LG domains bind to α-dystroglycan. To test this binding, we prepared recombinant pikachurin LG domains (residues 391–1,017) as a His-tag protein (pikachurin-LG–His) and recombinant α-dystroglycan as an Fc-fusion protein (DG-Fc). Pikachurin-LG–His was recovered in the NP-40–solubilized cell lysate. DG-Fc and its control Fc proteins were secreted into the cell culture media when expressed in NIH 3T3 cells. We confirmed that DG-Fc was recognized by a monoclonal antibody (IIH6) against glycosylated forms of α-dystroglycan (data not shown). We prepared DG-Fc–protein A beads, which were then mixed with the cell lysate that contained pikachurin-LG–His. The binding reaction was carried out in the presence of Ca^{2+} and Mg^{2+} or EDTA, as binding between α-dystroglycan and agrin or perlecan requires divalent cations[10,32,33]. Western blotting analysis of the bound materials using antibody to His revealed that the pikachurin LG domains bind to DG-Fc (**Fig. 6g**). This binding was inhibited by EDTA (**Fig. 6g**), which indicates that there is a divalent cation-dependent interaction, as is the case of laminin, agrin and perlecan[31]. We confirmed that pikachurin-LG–His did not bind to the Fc protein (**Fig. 6g**). In addition, the inhibitory effects of IIH6 (**Fig. 6h**) suggest that the pikachurin binding to α-dystroglycan is glycosylation-dependent, as IIH6 is reported to inhibit binding of laminin and perlecan[33,34]. Both

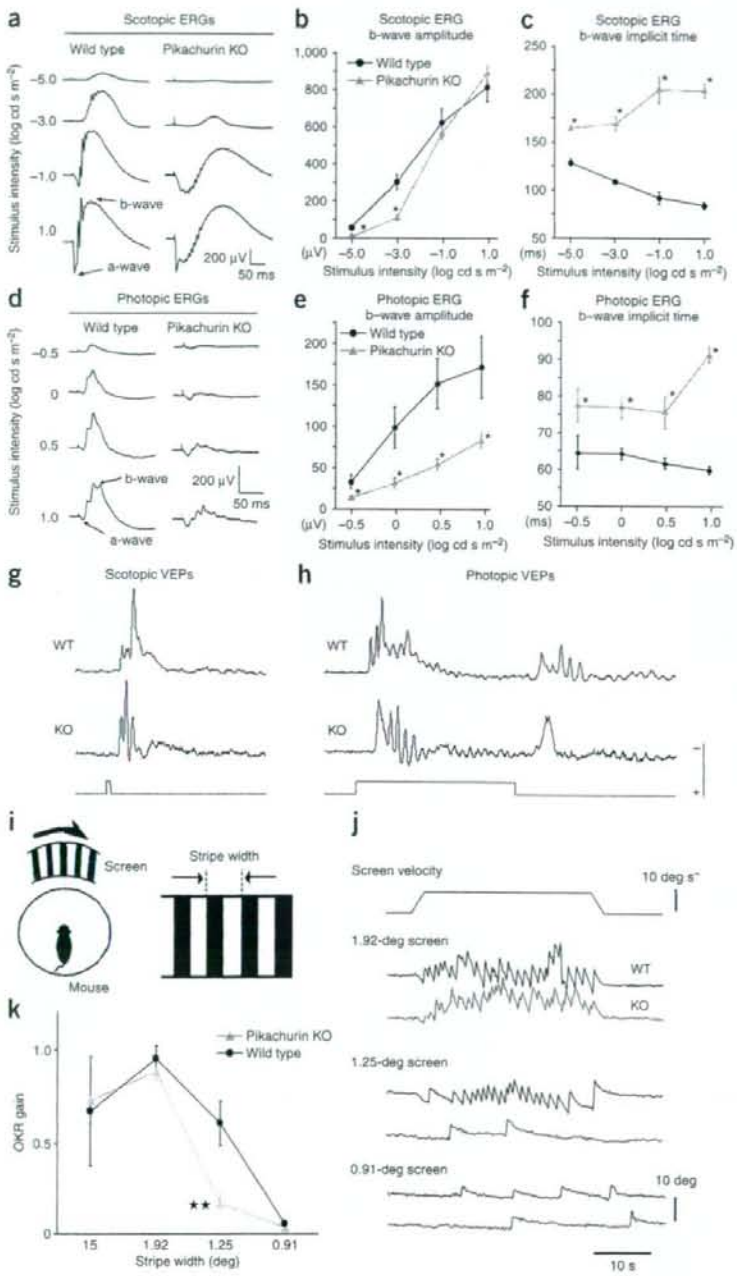

Figure 5 Electrophysiological and OKR analyses of wild-type and *Pikachurin* null mice. (**a–f**) ERG analysis of *Pikachurin*$^{-/-}$ mice. Scotopic (**a**) and photopic (**d**) ERGs were elicited by four different stimulus intensities from both wild-type and *Pikachurin*$^{-/-}$ (KO) mice ($n = 4$). Amplitude (**b**) and implicit time (**c**) of scotopic ERG b-waves as a function of the stimulus intensity are shown. Amplitude (**e**) and implicit time (**f**) of photopic ERG b-waves are shown. The bars indicate s.e.m. Asterisks indicate that the differences are statistically significant (Mann-Whitney test, $P < 0.05$). (**g,h**) VEPs in the superior colliculus of wild-type (WT) and *Pikachurin*$^{-/-}$ (KO) mice. (**g**) Under scotopic conditions, a brief 10-ms stimulation was applied from the LED panel (238 cd m^{-2}) in the front of the left eye. (**h**) Under photopic condition, a 500-ms stimulation was applied to examine both ON and OFF responses. The bottom trace indicates the onset and offset of a light stimulus. Scale bar indicates 200 μV. (**i–k**) OKR analysis of wild-type and *Pikachurin*$^{-/-}$ mice. A schematic drawing of OKR recording (**i**). (**j**) Screen velocity, scale bar represents 10° s^{-1}. Examples of OKRs in wild-type (black) and *Pikachurin*$^{-/-}$ (gray) mice with a 1.92-, 1.25- or 0.91-deg screen. (**k**) OKR gain with four screens of different stripe width. Bar indicates s.d. (gray triangle, *Pikachurin*$^{-/-}$ mice; black circle, wild-type mice, $n = 6$). OKR of *Pikachurin*$^{-/-}$ mice with 1.25-deg screen was significantly weaker than that of wild-type mice (unpaired t test, $P < 0.01$).

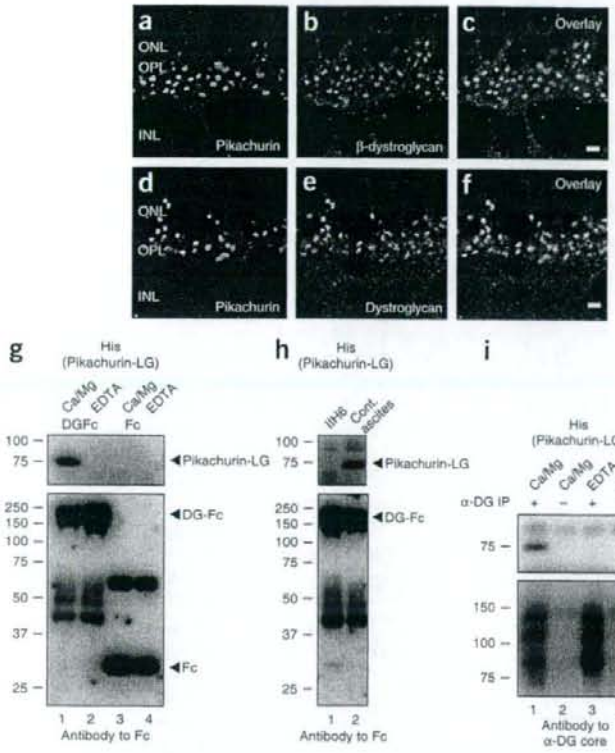

Figure 6 Interaction and colocalization of pikachurin with dystroglycan. (**a–f**) Confocal images of OPLs that were double labeled with antibodies to pikachurin (red, **a**,**d**) and β-dystroglycan (green, **b**) or dystrophin (green, **e**), showing that pikachurin colocalized with DGC molecules (**c**,**f**). Scale bars represent 2 μm. (**g**) Molecular interaction between pikachurin and α-dystroglycan. DG-Fc (lanes 1 and 2) or Fc (lanes 3 and 4) proteins were coupled with protein A beads and incubated with cell lysates containing pikachurin-LG–His in the presence of Ca^{2+} and Mg^{2+} (lanes 1 and 3) or EDTA (lanes 2 and 4). Bound materials were analyzed by western blotting with antibody to His tag (upper). A comparable amount of DG-Fc or Fc proteins on protein A beads were confirmed by staining with an antibody to Fc (lower). (**h**) Inhibitory effect of IIH6 on the interaction between pikachurin and α-dystroglycan. The binding reaction was carried out with (lane 1) or without (lane 2) the monoclonal antibody to α-dystroglycan IIH6. IIH6 selectively recognized glycosylated forms of α-dystroglycan. (**i**) Pikachurin interaction with eye α-dystroglycan. Native α-dystroglycan was immunoprecipitated from mouse eye extracts with antibody to α-DG core protein (lanes 1 and 3). For negative controls, antibody to α-DG core protein was omitted (lanes 2 and 4). The eye α-DG–protein G beads were tested for pikachurin binding in the presence of Ca^{2+} and Mg^{2+} (lanes 1 and 2) or EDTA (lanes 3 and 4). The samples were analyzed by western blotting with antibodies to His tag and α-DG core.

laminin and perlecan require α-dystroglycan glycosylation, which is recognized by IIH6, for binding to α-dystroglycan[35]. These data provide evidence of a direct interaction between pikachurin and α-dystroglycan.

To confirm the physiological interaction between pikachurin and α-dystroglycan in the retina, we carried out a pull-down assay using dystroglycan purified from murine retina. α-dystroglycan was immunoprecipitated from an eye extract using a specific antibody and assayed for an interaction with pikachurin. Consistent with our results using the recombinant α-dystroglycan, α-dystroglycan purified from murine eye interacts with pikachurin in a divalent cation–dependent manner (**Fig. 6i**). Furthermore, immunofluorescence analysis showed colocalization of pikachurin with both dystroglycan and dystrophin in the OPL (**Fig. 6a–f**), suggesting that pikachurin is a physiological ligand of α-dystroglycan in the retina.

DISCUSSION

Functional roles of *Pikachurin* in ribbon synapse formation

Structurally, synapses are specialized sites of cell-cell contact. Cell adhesion molecules and ECM proteins have been suspected, and in some cases have been demonstrated, to be important in synapse development and plasticity. In *Drosophila*, N-cadherins on both photoreceptor cells and their target neurons in the optic neuropil are required for proper target selection[36]. In vertebrates, however, cadherins do not seem to function in target recognition[37]. Agrin, an ECM molecule, has been extensively studied and proven to be required for postsynaptic differentiation, especially clustering of acetylcholine receptors, of the neuromuscular junction (NMJ)[38]. However, the effect and function of these cell adhesion and ECM molecules in synapse formation in the vertebrate CNS remain poorly understood. In the current study, our results demonstrate that a previously unknown ECM-like protein, pikachurin, is essential for proper bipolar dendritic tip apposition to the photoreceptor ribbon synapse. Notably, in the *Pikachurin* null retina, the tips of the bipolar cell dendrites are absent in photoreceptor ribbon synapse, but the horizontal cell terminus is not substantially affected. Immunostaining with antibody to mGluR6 or PKC in *Pikachurin* null retina did not show substantial differences in bipolar morphology (**Fig. 4l,m**), suggesting that bipolar cell differentiation is not perturbed. ERG studies showed that synaptic signal transmission from photoreceptors to bipolars was substantially prolonged but not lost. This suggests that the tips of the bipolar cell dendrites do not enter the invagination of photoreceptor terminals but still exist some distance apart from the ribbon synapse. This phenotype may be due to supporting molecules involved in photoreceptor-bipolar interaction, although pikachurin has a major role. Does the absence of the bipolar cell dendrite tips in the photoreceptor synapse occur because of a developmental defect or a maintenance abnormality after a normal synapse develops? Dynamic *Pikachurin* expression in developing photoreceptors (**Fig. 1d–g** and **Supplementary Fig. 1**) suggests that this phenotype is the result of developmental defects.

In this study, we focused our analysis on rod photoreceptor synapses (**Fig. 4a–k**), as the very small number of cones makes analysis with enough numbers of samples extremely difficult. However, several micrographs of cone synaptic terminals (**Supplementary Fig. 4**) and ERG results (**Fig. 5d–f**) suggest that similar synaptic abnormality probably occurs in cone photoreceptor synapses as was observed in rods. Typical ribbon synapses also exist in bipolar cell terminals in

retinal IPL and hair cells in the inner ear. Pikachurin expression was not detected in these sites, suggesting that pikachurin functions specifically in photoreceptor-bipolar synaptic apposition.

The human *PIKACHURIN* gene is located on chromosome 5, region p13.2-p13.1. Although human *PIKACHURIN* maps in the vicinity of early-onset autosomal dominant macular dystrophy (MCDR3), which was mapped to chromosome 5, region p13.1-p15.33 (RetNet, http://www.sph.uth.tmc.edu/Retnet/), *PIKACHURIN* mutations do not seem to be responsible for this disease when the phenotypes of the *Pikachurin* null mouse are taken into consideration. Notably, the *Pikachurin* null mouse showed an impairment of visual function detected by OKR (**Fig. 5i–k**). *Pikachurin* null mice showed normal visual function for large-angle stripes but significantly reduced visual function for small-angle stripes (unpaired t test, $P < 0.01$). This may suggest that a mutation of *PIKACHURIN* in humans leads not to an obvious clinical manifestation of eye disease but rather to impairment of spatial resolution in vision.

Functional interaction between pikachurin and dystroglycan

Our observations suggest the possibility of a functional interaction between pikachurin and dystroglycan (**Supplementary Fig. 6** online). We observed a reduction in the amplitude and delayed implicit time of the ERG b-wave (**Fig. 5a–f**) in the *Pikachurin*$^{-/-}$ mouse. Both in human and mouse, mutations of dystrophin, an intracellular component of the DGC, are known to cause an abnormality in the ERG b-wave. In humans, many individuals with DMD and BMD with mutations in dystrophin show abnormal dark-adapted ERG b-waves[17,28]. Studies of individuals with DMD deletions have shown that the location of the deleted sequence can affect the ERG phenotype[29]. Mutations in the central or 3′ region of the gene are associated with severe reductions of amplitude and prolongation of the implicit time in the b-wave, whereas mutations limited to the 5′ end of the gene appear to be associated with milder abnormalities and, in some cases, normal ERGs[29]. In mice, disruption of dystrophin (*mdx*^{Cv2} and *mdx*^{Cv4}) causes prolongation of the implicit time of the b-wave[18]. Our results suggest that functional disruption of the interaction between dystroglycan and pikachurin in the retina may produce abnormal dark-adapted ERG b-waves in individuals with DMD and BMD. In addition, lack of glycosylation of α-dystroglycan in glycosyltransferase-deficient mice (*Large*^{myd} and *Large*^{vls}) also shows an ERG phenotype that is similar to that of *Pikachurin* null mice[30]. The similarity of unique abnormalities of ERGs observed in the *Pikachurin* null, *mdx*^{Cv2}, *mdx*^{Cv4}, *Large*^{myd} and *Large*^{vls} mutants strongly suggest that there is a functional interaction between pikachurin and DGC components in the retinal ribbon synapses.

We also found a direct interaction of pikachurin with α-dystroglycan, an extracellular component of the DGC (**Fig. 6**). It has been reported that α-dystroglycan binds to laminins and perlecan in a glycosylation-dependent manner[35]. The inhibitory effect of IIH6 and divalent cation–dependent binding suggest that pikachurin binds to α-dystroglycan by a mechanism that is similar to other known ligands, such as laminins and perlecan. Supporting this idea, pikachurin colocalizes with β-dystroglycan in photoreceptor synaptic terminals (**Fig. 6a–c**).

On the basis of these data, pikachurin probably functionally interacts with DGC components to form proper synaptic connections between photoreceptors and bipolar cells in the retinal ribbon synapses.

Molecular mechanism of pikachurin in synapse formation

In NMJs, formation of the proper synaptic structure is regulated by several dystroglycan ligands, such as agrin, laminins and perlecan. These ligands interact with dystroglycan, localizing to the postsynaptic surface of NMJ, and induce the differentiation and maturation of postsynaptic structures through the clustering of appropriate postsynaptic components (**Supplementary Fig. 6**)[39,40]. In contrast to the postsynaptic localization of dystroglycan in NMJs, dystroglycan in the ribbon synapse localizes to the presynaptic membrane of photoreceptor synaptic terminals around the bipolar cell dendritic processes[12–14]. To the best of our knowledge, pikachurin is the first dystroglycan ligand that has been found to interact with the presynaptic dystroglycan (**Supplementary Fig. 6**). How does pikachurin control invagination by the bipolar dendritic tips of the photoreceptor presynaptic terminals? On the basis of our data and previous findings, we hypothesize two scenarios. The first scenario is that pikachurin is involved in forming the proper structure of photoreceptor terminals for invagination by the tips of bipolar dendrites. The interaction of pikachurin with dystroglycan on the surface of the presynapse may cause a structural change of the photoreceptor presynaptic terminals, forming the proper connection with the postsynaptic terminals of bipolar dendrites. This scenario leads to the hypothesis that fine structural conformation of the axon terminus is crucial for the initial specific and precise synaptic apposition of a dendrite to the axon terminus. After this, adhesive molecules function supportively for the successive development and maintenance of synaptic connections.

The second scenario is that pikachurin is an attractant that induces the bipolar dendritic tips into proximity with the photoreceptor ribbon synapse through interaction with an unknown factor (represented as a factor, X; **Supplementary Fig. 6**) on the postsynaptic terminals of bipolar cell dendrites. Pikachurin released from photoreceptor synapses may induce structural changes in bipolar dendritic tips, such as the clustering of postsynaptic components, via an interaction with the unknown factor expressed in the tips of the bipolar cell dendrites. This may result in the attraction and insertion of the bipolar dendritic tips to the invagination of photoreceptor synaptic terminals.

In this study, we demonstrated that a previously unknown dystroglycan-interacting protein, pikachurin, is important for the formation of the ribbon synapse, a specialized synaptic structure in the CNS. Dystroglycan is known to be expressed not only in muscular cells but also in various CNS neurons[41]. Our findings provide clues as to the mechanisms of dystroglycan and ECM molecules in the formation of fine CNS synaptic structures.

METHODS

Generation of *Pikachurin* mutant mouse. We obtained *Pikachurin* genomic clones from a screen of the 129/SvEv mouse genomic DNA library (Stratagene). We subcloned an 8.4-kb *SwaI-ScaI* fragment and an 8.1-kb *EcoRV-KpnI* fragment from the *Pikachurin* genomic clones into a modified pPNT vector[42], and transfected the linearized targeting construct into TC1 embryonic stem cell line[42]. The culture, electroporation and selection of TC1 were carried out as previously described[42]. Embryonic stem cells that were heterozygous for the targeted gene disruption were microinjected into C57BL/6 blastocysts to obtain chimeric mice.

We carried out immunohistochemistry, northern blot analysis, RT-PCR analysis, *in situ* hybridization, electron microscopy, ERG recordings, VEP recording, OKR analysis and pull down binding assays as described in the **Supplementary Methods** online.

Note: Supplementary information is available on the Nature Neuroscience website.

ACKNOWLEDGMENTS

We thank Y. Kambara, M. Murai, T. Tsujii, E. Oiki, S. Takiuchi and K. Sone for technical assistance; Y. Saijoh, M. Uehara and H. Hamada for advice on the production of a knockout mouse; and N. Maeda for statistical analysis. This work was supported by Molecular Brain Science, Grant-in-Aid for Scientific